Earth and Planetary Science Letters 433 (2016) 192–203

Contents lists available at ScienceDirect

Earth and Planetary Science Letters

www.elsevier.com/locate/epsl

Tracking the provenance of Greenland-sourced, Holocene aged, individual sand-sized ice-rafted debris using the Pb-isotope compositions of feldspars and $^{40}Ar/^{39}Ar$ ages of hornblendes

Lee F. White[a,*], Ian Bailey[b,*,1], Gavin L. Foster[b], Georgina Allen[b,2], Simon P. Kelley[c], John T. Andrews[d], Kelly Hogan[e,3], Julian A. Dowdeswell[e], Craig D. Storey[a]

[a] School of Earth and Environmental Sciences, University of Portsmouth, Burnaby Road, Portsmouth PO1 3QL, UK
[b] Ocean and Earth Science, National Oceanography Centre Southampton, University of Southampton, European Way, Southampton SO14 3ZH, UK
[c] Department of Environment, Earth and Ecosystems, The Open University, Milton Keynes MK7 6AA, UK
[d] INSTAAR and Department of Geological Sciences, University of Colorado, Boulder, CO 80309, USA
[e] Scott Polar Research Institute, University of Cambridge, Lensfield Road, Cambridge, CB2 1ER, UK

ARTICLE INFO

Article history:
Received 23 April 2015
Received in revised form 30 October 2015
Accepted 31 October 2015
Available online 12 November 2015
Editor: D. Vance

Keywords:
Greenland
ice rafted debris
Ar–Ar
Pb isotopes
icebergs
provenance

ABSTRACT

The provenance of sand-sized ice-rafted debris (IRD) sourced from Greenland is currently difficult to determine. Such knowledge, if it could be ascertained with a high degree of certainty, could be applied to the Greenland-proximal marine records to improve both our understanding of modern-day spatial patterns of iceberg rafting and the past history of the Greenland Ice Sheet (GIS). Recent studies have highlighted the utility of the Pb-isotope composition of individual sand-sized feldspars and the $^{40}Ar/^{39}Ar$ ages of individual sand-sized hornblendes in this regard. However, before any such provenance toolkit can be applied to the palaeo-record, it is necessary first to determine whether this approach can be used to track the sources of known recent Greenland-proximal IRD deposition. To this end we present new records of the Pb-isotope composition and the $^{40}Ar/^{39}Ar$ ages of individual sand-sized grains of feldspars and hornblendes, respectively, from modern Greenland glacifluvial and fjord sands and Holocene to modern Greenland-proximal marine sediments. These new data demonstrate that sand-sized feldspars and hornblendes glacially eroded by the GIS exhibit distinct intra- and inter-tectonic terrane differences in their Pb-isotope compositions and ages and that these differences are clearly expressed in the geochemistry and geochronology of sand-sized IRD deposited in marine sediments around Greenland. Although overlap exists between some Greenland-proximal IRD 'source fields' defined by these data, our approach has the potential to both better understand spatial patterns of Greenland-derived IRD in the modern day as well as during past episodes of iceberg calving.

1. Introduction

The Arctic is one of the fastest warming regions on Earth (Bindoff et al., 2013). It also includes the Greenland Ice Sheet (GIS), which, if it were to melt completely, would contribute ~7.3 metres of global sea-level rise (Meehl et al., 2007). Understanding how the GIS will respond to anthropogenically-induced global warming over the coming century is therefore important. This need is further highlighted by the fact that glacial isostatic adjustment complicates accurate prediction and associated mitigation since the impact of deglaciation of the GIS and the West Antarctic Ice Sheet (also under threat from future melt-reduction and/or collapse; Carlson and Winsor, 2012) on sea-level would be felt differently in both near and far field regions (e.g. Mitrovica et al., 2009).

Current scenarios depicting the extent to which the GIS will deglaciate in response to future warming are heavily dependent on the capabilities of numerical climate models, which are embedded with large uncertainties (i.e. Otto-Bliesner et al., 2006). The current generation of climate models lack the capacity to accurately model melt- and growth-histories and basal dynamics of

* Corresponding authors.
E-mail addresses: Lee.White@port.ac.uk (L.F. White), I.Bailey@exeter.ac.uk (I. Bailey).

[1] Present address: Camborne School of Mines, University of Exeter, Penryn Campus, Cornwall TR10 9FE, UK.

[2] Present address: Mouchel, 37–39 Perrymount Road, Haywards Heath, West Sussex RH16 3DN, UK.

[3] Present address: British Antarctic Survey, Madingley Road, High Cross, Cambridge, CB3 0ET, UK.

http://dx.doi.org/10.1016/j.epsl.2015.10.054

continental ice-sheets (Morlighem et al., 2014). To improve prediction of the likely response of the GIS to future warming it is therefore necessary to ground truth model output by simulating continental ice-sheets for a variety of past climates and comparing the results with geological observations (e.g. Thiede et al., 2011; Reyes et al., 2014). Another approach, however, would be to improve our understanding of the dynamic range of the GIS and possibility for threshold melt-reduction behaviour as a function of radiative forcing (due to changes in, e.g., boreal summer insolation and atmospheric CO_2) from an empirical-data perspective by reconstructing the GIS from the geological record for a variety of past warmer and colder-than-present climate states (e.g. Thiede et al., 2011; Reyes et al., 2014).

Reconstructions of the Holocene history of the GIS have considerably advanced our understanding of the relationship between GIS retreat and radiative forcing associated with the last deglacial. Such studies have benefited from an abundance of spatially diverse geological evidence recorded within both terrestrial (e.g. Bennike and Björck, 2002; NGRIP, 2004; Dyke et al., 2014; Winsor et al., 2015) and GIS-proximal marine (e.g. Knutz et al., 2011; Hogan et al., 2012; Knutz et al., 2013) realms, and reveal that the spatial extent of the GIS reached a minimum by the early Holocene (∼11–7 ka) during peak boreal summer insolation. Our ability, however, to estimate the likely response of the GIS to radiative forcing under future projections for atmospheric CO_2 is limited by insufficient geological-based evidence for GIS extent during older deglacials and interglaciations. Recently, evidence in the form of seismic studies (Nielsen and Kuijpers, 2013; Knutz et al., 2015), the provenance of silt-sized terrigenous sediments discharged from southern Greenland to Eirik drift (Reyes et al., 2014) and ^{10}Be measurements on silt from the bottom of the central Greenland GISP2 ice core (Bierman et al., 2014) has provided new insights into the past history of the GIS prior to the Holocene. One currently underutilised, but complimentary, approach that could be used to enhance our understanding in this respect is to examine the provenance of individual sand-sized ice-rafted debris (IRD) deposited in Greenland-proximal marine settings to estimate past locations of GIS iceberg calving and drift.

The Pb-isotope compositions and ^{40}Ar/^{39}Ar ages of individual sand-sized feldspars (Gwiazda et al., 1996; Bailey et al., 2012) and hornblendes (Hemming et al., 1998; Knutz et al., 2013), respectively, have proven useful for tracking sources of ice-rafted sediments. Our current understanding of the potential sources for sand-sized ice-rafted hornblendes and feldspars derived from Greenland is based on knowledge of only the age ranges assigned to individual tectonic terranes (Fig. 1) and on a geographically incomplete compilation of the Pb-isotope compositions of feldspars and ore galenas from bedrock samples (Gwiazda et al., 1996; Bailey et al., 2012). Little is known, however, about the age distribution and Pb-isotope composition of individual sand-sized hornblendes and feldspars preferentially incorporated into icebergs sourced from specific iceberg-calving locations on Greenland today (Rignot and Kanagaratnam, 2006). To address this gap in our knowledge, we report the Pb-isotope composition of individual feldspars and the ^{40}Ar/^{39}Ar ages of individual hornblendes from Greenland glacifluvial sands collected from a series of modern-day sandurs close to a geographically diverse range of iceberg calving locations. In doing so we address the following related questions: 1) What range and diversity exists in the Pb isotope composition and age of IRD incorporated into icebergs from specific GrIS calving source regions? 2) What is the Pb isotope composition and age of IRD deposited during the Holocene in Greenland-proximal marine sediments? 3) To what extent can we use such data to reconstruct the provenance of Holocene to modern Greenland-proximal IRD deposition?

2. Geology of Greenland and its major modern iceberg calving sources

Greenland consists of a number of tectonic terranes bearing metamorphic ages ranging from 3.9 Ga to 390 Ma (Fig. 1; Dawes, 2009). The geology of central and southern Greenland is predominantly Precambrian in age and is divided into three regions: the Ketilidian Mobile Belt (KMB), the Archaean Block (AB) and the Nagssugtoqidian Mobile Belt (NMB) (i.e. Henriksen et al., 2009) (Fig. 1). The AB is primarily composed of Neoarchaean orthogneisses (2.6–3.1 Ga), although Eoarchaean orthogneisses, up to 3.9 Ga in age, occur locally in the region of Nuuk whilst paragneisses, ∼3.8 Ga in age, occur within the Isua Supracrustal Belt (Henriksen et al., 2009). The NMB is an area that is interpreted to represent a reworked marginal portion of the AB as the result of a Palaeoproterozoic (1.7–1.9 Ga) metamorphic overprint. This area lies north of ∼65°N, and comprises the Ammassalik terrane and Nagssugtoqidian orogeny (Connelly and Thrane, 2005). In central west Greenland, in the region around Disko Bugt, the NMB is characterised by the Rinkian fold belt, a several kilometre thick Palaeoproterozoic succession inter-folded with reworked Archaean gneiss (Grocott and Pulvertaft, 1990). The KMB defines the southern-most tip of Greenland and is composed of granitoids and low- to high-grade metasediments formed within the time period ∼1.9–1.7 Ga (Henriksen et al., 2009).

Coastal eastern Greenland contains a mountain range that is a relic of the Lower Palaeozoic Caledonian orogeny, composed of thrust sheets and local eclogites within reworked Palaeoproterozoic basement gneisses that formed ∼390–410 Ma ago (i.e. Gilotti et al., 2008) (Fig. 1). The southern region of the Caledonides in the area of Scoresby Sund comprises granodioritic and dioritic plutons that yield intrusive ages of 420–466 Ma (Kalsbeek et al., 2008). The northernmost granites yield intrusion ages of 425–430 Ma (Strachan et al., 2001). Caledonian rocks of Scoresby Sund are separated from NMB rocks outcropping in the region of the Kangerlussuaq Fjord System by Cenozoic basaltic volcanics of the Geikie Plateau (Fig. 1).

Today, major iceberg-calving sources are located in Disko Bugt in the western NMB (∼34.8 km^3/yr) and the Scoresby Sund Fjord system in the east Caledonides (∼13.2 km^3/yr) (Fig. 1), with these two sources alone contributing ∼13% to the total annual GIS iceberg flux (Weidick, 1995; Rignot and Kanagaratnam, 2006). In east Greenland, the Geikie Plateau supplies the dominant lithic fragments found in sediments deposited in the nearby Kangerlussuaq trough (Alonso-Garcia et al., 2013; Andrews et al., 2014a). Other notable NMB iceberg sources in this region include multiple tidewater glaciers in the Kangerlussuaq Fjord System (∼28 km^3/yr) and regions south thereof, including the Hutchinson Plateau, Uunartit Island and Helheimgletscher at the head of Sermilik Fjord (∼23–26 km^3/yr; Rignot and Mouginot, 2012) (Fig. 1). The AB is a source of relatively high volumes of icebergs along the southeast (∼46–67 km^3/yr, ∼13–19%; Rignot et al., 2004; Rignot and Kanagaratnam, 2006) and southwest (∼60 km^3/yr; ∼17%) coasts of Greenland including notable contributions from Eqalorutsit Killiit Sermiat near Nuuk (∼6–11.5 km^3/yr) and Ukaasorsuaq glacier in Sermilik Fjord (∼6–12 km^3/yr; Weidick and Bennike, 2007) (Fig. 1).

The East Greenland Current (EGC) exports icebergs from east Greenland clockwise along the landward side of the Denmark Strait (Fig. 1). Along the southern tip of Greenland the West Greenland Current (a mixture of EGC and the relatively warmer North Atlantic Irminger Current) circulates icebergs calved locally from the KMB (notably Qajuuttap Sermia and Eqalorutsit Killiit Sermiat tidewater glacier systems at the head of Nordre Sermilik Fjord near Narssarsuaq (∼6 km^3/yr; Weidick and Bennike, 2007; Rignot and Kanagaratnam, 2006) in a northerly direction along the

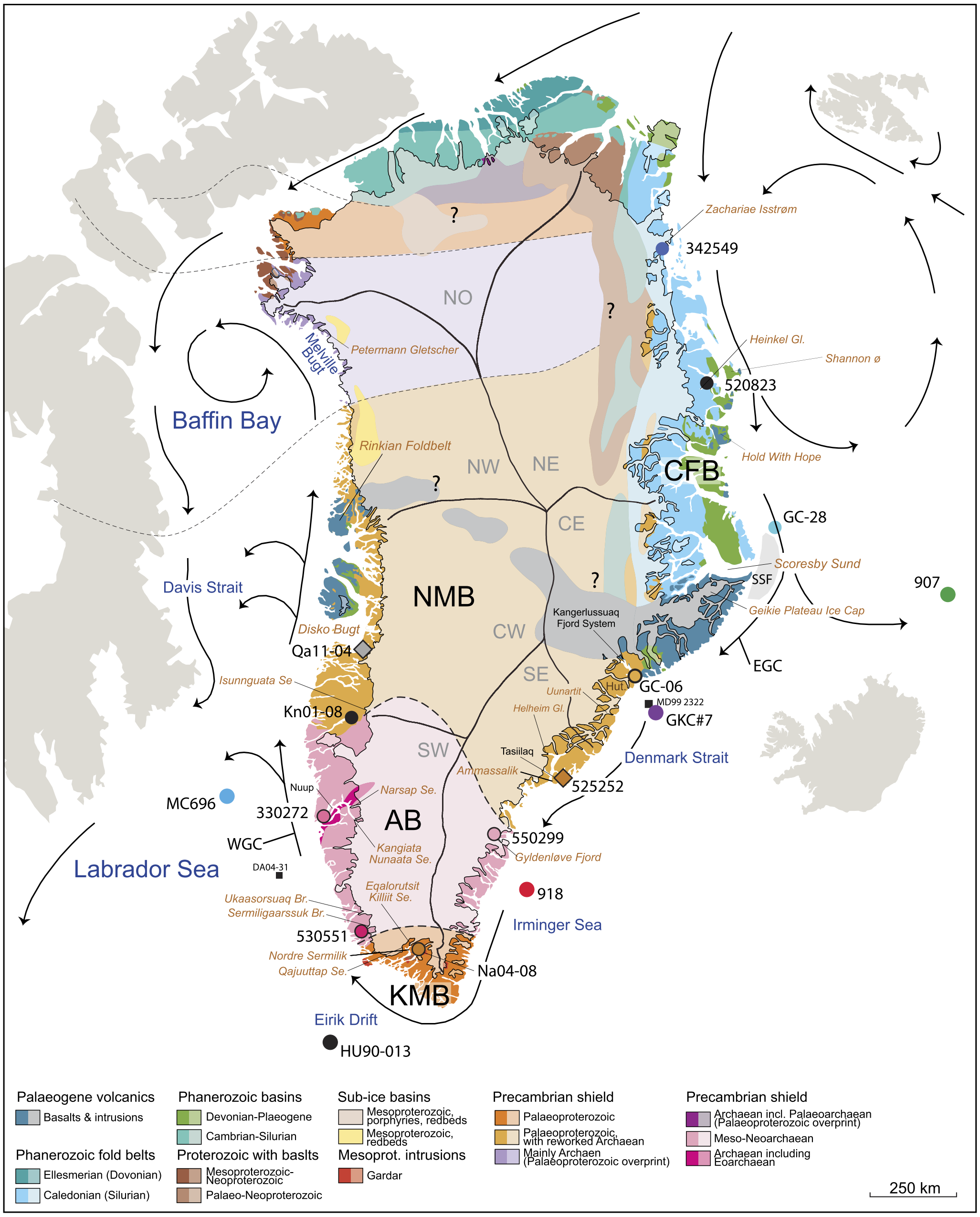

Fig. 1. Geological map of Greenland with interpretation of sub-ice bedrock modified from Dawes (2009; their Fig. 1). Ice-free geology at coast is illustrated by darker coloured shading. KMB = Ketilidian Mobile Belt, AB = Archaean Block, NMB = Nagssugtoqidian Mobile Belt, CFB = Caledonian Fold Belt. Also shown are terrestrial and marine study sites referred to in the main text (and detailed in Table 1), as well as major glacier/fjord systems (brown text) and ice sheet divides (black lines) (Weidick, 1995). Major drainage regions are labelled as NO = North, NE = North East, CE = Center East, SE = South East, SW = South West, CW = Center West, NW = North West. Br. = Bræ, Gl. = Glacier, and Se. = Sermia. Black arrows denote simplified modern day current systems. E/WGC = East/West Greenland Current. SSF = Scoresby Sund Fan. Hut. = Hutchinson Plateau Ice Cap. (For interpretation of the references to colour in this figure legend, the reader is referred to the web version of this article.)

West Greenland coast, where they mix with icebergs calved from the western AB in the Labrador Sea, through eastern Davis Strait and potentially on into Baffin Bay (Fig. 1). Icebergs from Disko Bugt may travel northwards into Baffin Bay, but preferentially move westwards and southwards through western Davis Strait and further south into the Labrador Sea, and occasionally into waters off Newfoundland (Bigg et al., 1996; Tang et al., 2004) (Fig. 1). Within eastern Disko Bugt calved ice preferentially moves northwards, though a number of smaller icebergs are known to move westwards into the Davis Strait (Valeur et al., 1996). Today, the Canadian Archipelago (e.g. Baffin and Ellesmere Islands) does not represent a significant source of IRD to Baffin Bay (Tang et al., 2004).

IRD sourced from northeast Greenland and from sea–ice exported from the Siberian coast of Russia by the Transpolar Drift (Pfirman et al., 1997) are also transported southwards towards our study region by the EGC. Whilst such material represents potential distal sources of IRD deposited at our study sites, their contribution is likely to be low. Though sea–ice is sand-poor (Dethleff and Kuhlmann, 2009), recent XRD-based studies of the <2 mm fraction of terrigenous sediments from Baffin Bay (Andrews et al., 2014b), the western Nordic Sea (Andrews and Vogt, 2014) and on Denmark Strait (Andrews, 2011) indicate that IRD deposited in these regions during the modern and the Late Quaternary is sourced mainly from local glacial erosion, consistent with iceberg modelling studies (Bigg et al., 1996). These observations suggest that the spatial

Table 1
Terrestrial and Greenland-proximal marine samples used in this study.

Sample ID	Locality/region	Grid ref.	Water depth (m)	Greenland terrane	Glacier system(s)*	Feldspar analyses	Hornblende analyses
Na04-08	Nordre Sermilik Fjord, Narssarsuaq,	61.1′N, 45.2′W	River Sand	KMB	Qajuuttap Sermia, Eqalorutsit Killiit Sermiat	6	–
530551	Sermiligaarssuk Fjord	61.5′N, 48.3′W	River Sand	Western AB	Sermiligaarssuk Br., Sioralik Br.	20	25
330272	Nuup Kangerlua River, Nuuk	64.2′N, 51.5′W	River Sand	Western AB	Kangilinnguata Sermia, Narsap Se., Qamanaarsuup Se., Akullersuup Se., Kangiata Nunaata Se.	24	25
550299	Gyldenløve Fjord	64.2′N, 41.2′W	River Sand	Eastern AB	unnamed Gls.	16	25
Kn01-08	Kangerlussuaq Fjord	67.1′N, 50.4′W	River Sand	Western NMB	Isunnguata Se., Russell Gl.	24	–
Qa11-01	Disko Bugt	68.3′N, 50.5′W	River Sand	Western NMB	Jakobshavn Isbrae, Alangorliup & Saqqarliup Se.	34	10
525252	Kuummiit (Tasiilaq)	65.7′N, 36.7′W	River Sand	Eastern NMB	Knud Rasmussen Gl., Kaarale Gl.,	12	–
Site JR106-GC06 1W 1–3 cm	Mouth of Kangerlussuaq Fjord System	68.1′N, 32.1′W	877	Eastern NMB	Kangerlussuaq, Coultard, Styrtegletscher, Nordfjord and Frederiksborg Gls.	20	5
342549	Zachariae Isstrøm	78.4′N, 20.4′W	River Sand	CFB	Zachariae Isstrøm	30	24
520823	Near Hochstetterbugten, Østgrønland	74.7′N, 21.6′W	River Sand	CFB	Heinkel Gl.	12	–
Site JR51-GC28 1–2 cm	Immediately north of Scoresby Sund Fan	71.1′N, 18.3′W	1600	–	Offshore	21	–
Site 918A 1H 1W 37–39 cm	Irminger Basin	63.5′N, 38.4′W	1880	–	Offshore	35	8
Site MC696, 0–1.5 cm	Labrador Sea	64.0′N, 57.6′W	n/a	–	Offshore	18	10
Site HU-90-013-013, 2–4 cm	Eirik Drift	58.1′N, 48.2′W	3771	–	Offshore	36	10
Site 907A 1W 31–33 cm	Iceland Plateau	69.1′N, 12.4′W	1811	–	Offshore	24	–
PO175GKC#7 1–2 cm	Denmark Strait (outer Kangerlussuaq Trough)	66.6′N, 30.8′W	300	–	Offshore	28	–

KMB = Ketilidian Mobile Belt, AB = Archaean Block, NMB = Nagssugtoqidian Mobile Belt, CFB = Caledonian Fold Belt. Br. = Bræ, Gl. = Glacier, and Se. = Sermia.
[*] After Rignot and Mouginot (2012). Marine sediment examined is either core top sediment (i.e. modern) or deposited on Eirik Drift[a] during the latest Holocene (Vernal and Hillaire-Marcel, 2000), in the Irminger Basin[b] during the middle Holocene, ∼6 ka (St John and Krissek, 2002), on the Iceland Plateau[c] during the early Holocene, ∼10 ka (Jansen et al., 2000) and in the Kangerlussuaq Trough over the past 150 yr (Alonso-Garcia et al., 2013).

pattern of IRD deposition in marine-proximal Greenland settings is dominated by local sources and that any far-travelled ice and its IRD are therefore diluted during sediment deposition by local glacial meltwater plumes and iceberg calving. This study therefore moves forward on the assumption that to identify the full range of iceberg calving sources on Greenland for any given time slice requires analysis of IRD deposited at a widely distributed network of marine sites.

3. Materials and methods

3.1. Study sites

This study examines the provenance signature of individual feldspars and hornblendes from river and fjord sands collected from eleven widely distributed locations on the western, eastern and southern margins of south Greenland and that of sand IRD deposited in the modern or Early to Late Holocene at five Greenland-proximal marine locations (Table 1; Fig. 1). Limited Pb-isotope data exist for individual feldspars in bedrock from the Palaeoproterozoic Nagssugtoqidian orogen in Disko Bugt and the Rinkian fold belt (Connelly and Thrane, 2005), which are used here to gain a first order insight into the Pb isotope composition of feldspars ice-rafted from these regions. To better understand potential heterogeneity in the provenance character of iceberg calving sources we prefer, however, to study the Pb-isotope compositions and $^{40}Ar/^{39}Ar$ ages of individual sand-sized grains in glacifluvial and/or marine-proximal (fjord) sediments, as opposed to isolated bedrock specimens, since the former record an integrated signal of subglacial erosion within a particular drainage basin which will better represent that incorporated into calved icebergs.

Glacifluvial samples were targeted with modern iceberg sources in mind (Table 1). Samples Qa11-01 and Kn01-08 (Table 1) from the western NMB were targeted to characterise the provenance signature of modern-day sources of Greenland icebergs and IRD, respectively, in Disko Bugt (which housed the Last Glacial fast flowing Jakobshavn ice stream; Hogan et al., 2012) and the region south of that (Fig. 1). Glacifluvial sand '525252' sampled proximally to the east of Kuummiit (near Tasiilaq) is used to define the provenance signature of Kaarale and Knud Rasmussen Glaciers on the eastern coast of the NMB. Core top sediment from Site JR106-GC06 is also used from this region for the provenance signature of IRD sourced from the Kangerlussuaq Fjord System (Dowdeswell et al., 2010). Sample Na04-08 from Nordre Sermilik Fjord near Narssarsuaq is used to characterise the provenance of KMB-sourced IRD from southernmost Greenland. Glacifluvial sands '330272' and '530551' are used here to capture the provenance character of AB-sourced IRD calved from the Kangiata Nunaata (Nuuk) and Sermiligaarssuk and Sioralik tidewater glaciers on the southwest coast of Greenland. Northeast Greenland glacifluvial sands '520823' (Østgrønland) and '342549' (Zachariae Isstrøm) and sediments from Site JR51-GC28 recovered by piston coring of the region just north of the Scoresby Sund Fan were also analysed to characterise IRD derived from East and Northeast Greenland outlet glaciers.

To understand spatial differences in the provenance of IRD deposited in marine settings proximal to Greenland, core-top or Holocene-aged sediments were examined from the Iceland Plateau (Ocean Drilling Program, ODP, Site 907), East Greenland Shelf (Site PO175-GKC#7), Irminger Sea (ODP Site 918), Eirik Drift (Site HU-90-013-013) and the Labrador Sea (Site MC-696) (large coloured circles, Fig. 1). The ages of samples from Sites 907 and 918 (∼10 ka and ∼6 ka, respectively; Table 1) were determined by reference to published age models for their stratigraphies (Jansen et al., 2000; St John and Krissek, 2002). IRD examined from the East Greenland shelf above Denmark Strait, Eirik Drift and the Labrador Sea comes from either core top (i.e. modern) sediments or was deposited in the latest Holocene (Table 1).

3.2. Individual feldspar and hornblende analyses

The $^{40}Ar/^{39}Ar$ dating of hornblendes and Pb-isotope analysis of feldspars has proven useful for tracking the sources of IRD deposited in the North Atlantic Ocean (e.g. Gwiazda et al., 1996; Hemming et al., 1998; Bailey et al., 2013; Knutz et al., 2013) and the Southern Ocean (e.g. Cook et al., 2014). Unlike accessory minerals used in tectonic provenance research (e.g. zircons for U–Pb/Hf dating or apatites and titanites for Sm–Nd isotopes), our target grains are common in both fluvial and clastic-rich marine sediments.

3.2.1. Pb isotopes in individual sand-sized feldspars

Pb-isotope analyses ($n = 363$; Table 1) of individual sand-sized (>150 μm) feldspar were performed at the University of Southampton on a Thermo-Scientific Neptune multicollector inductively coupled plasma mass spectrometer (MC-ICPMS) coupled with a NewWave/ESI UP193fx homogenised ArF excimer laser ablation system, operating at a wavelength of 193 nm, following methods reported in Bailey et al. (2012) (see Supplementary Materials). Feldspar grains were chosen randomly to best reflect the compositional variability within the sample, resulting in a natural preference towards K-feldspar (>80%) over plagioclase (∼20%), although analyses of both phases are henceforth referred to as 'feldspar'. Most ablations were performed with a laser spot size of 150 μm, with a small minority (<1%) analysed with a 100 μm spot. The Pb-isotope compositions of at least twenty grains were determined for each sample (Table 1). When initial analyses indicated the dominance of a single population less than 20 grains were analysed (e.g. Na04-08). Feldspar provenance is evaluated through their $^{206}Pb/^{204}Pb$ and $^{207}Pb/^{204}Pb$ ratios. No additional fidelity in provenance could be achieved by also using their $^{208}Pb/^{204}Pb$, $^{207}Pb/^{206}Pb$ and $^{208}Pb/^{206}Pb$ ratios (all Pb-isotope data are available in our Supplementary Materials).

3.2.2. $^{40}Ar/^{39}Ar$ ages of individual sand-sized hornblendes

Individual sand-sized (>150 μm) hornblende grains ($n = 142$; Table 1) were washed by ultrasonic treatment using deionised water and packaged within aluminium foil in preparation for neutron irradiation at the McMaster reactor (Canada). The $^{40}Ar/^{39}Ar$ ages of irradiated hornblendes were determined at the Argon Isotope Laboratory at the Open University (UK) using noble gas mass spectrometry following Sherlock (2001). Irradiated samples were loaded into the laser-extraction system, and individual hornblende grains were fused with an infrared ($\lambda = 1064$ nm) Nd-YAG laser or ablated for five minutes with an ultraviolet ($\lambda = 213$ nm) laser-ablation microprobe. Neutron flux was measured using biotite standard GA1550 (98.8 ± 0.5 Ma, Renne et al., 1998). Methods closely followed techniques for both ultraviolet (Wartho et al., 1999) and infrared (Adams and Kelley, 1988) analyses, including correction for measured blanks both before and after unknown sample analysis. Small sample sizes and low potassium led to high individual errors in some of the grains dated. All data are reported, but only data points with individual uncertainties of ≤ ∼3% (2 s.d.) are interpreted.

4. Results and discussion

4.1. Characterising the provenance signature of Greenland's ice-rafted debris

4.1.1. Pb isotopic composition of feldspars from Greenland fjord and glacifluvial sands

The Pb isotope ($^{206}Pb/^{204}Pb$ and $^{207}Pb/^{204}Pb$) compositions of 192 individual sand-sized feldspars from our target glacifluvial sands and fjord sediments from Greenland are shown in Fig. 2. A large range in Pb-isotope values is observed in these datasets, with a high degree of separation in Pb–Pb space between feldspars derived from each of Greenland's tectonic terranes. Compared with previous compilations of the Pb-isotope composition of these tectonic terranes based on bedrock data (Bailey et al., 2012), our new data demonstrate the significant extra fidelity that can be achieved for Greenland sand IRD provenance by examining glacifluvial sands (Fig. 3).

The Pb-isotope signature of the majority (95%) of feldspars derived from Scoresby Sund (JR51-GC28) and Disko Bugt (Qa11-01), the largest single modern-day iceberg calving sources on Greenland, are largely distinct in $^{206}Pb/^{204}Pb$ vs. $^{207}Pb/^{204}Pb$ cross plots (henceforth 206–207 space; compare Figs. 2A, D, E). Disko Bugt feldspars form a well-defined linear array in 206–207 space with $^{206}Pb/^{204}Pb$ ratios between ∼13 and 17 associated in turn with progressively increased $^{207}Pb/^{204}Pb$ ratios (Figs. 2D). In contrast, most feldspars ($n = 16$, 76%) from Scoresby Sund form a linear array with positive slope in 206–207 space with $^{206}Pb/^{204}Pb$ ratios between ∼17 and 19, although a small subset ($n = 5$, 24%) also form a separate, but tighter, array with $^{206}Pb/^{204}Pb$ spanning ∼14.5 to ∼16.5 (Fig. 2A). The signature of feldspars from the Scoresby Sund region (JR51-GC28) is highly comparable in 206–207 space to that which have been determined for Østgrønland (520823) and for Zachariae Isstrøm (342549) from further north (Fig. 1), although the lattermost source exhibits a significantly larger spread (of ∼17 to ∼21) for its most radiogenic $^{206}Pb/^{204}Pb$ isotope values when compared to our Scoresby Sund dataset (Figs. 2A, E).

Feldspars from Disko Bugt (Qa11-01) overlap in 206–207 space with other NMB datasets. For instance, the most unradiogenic Pb-isotope compositions ($^{206}Pb/^{204}Pb < 15$) of Disko Bugt feldspars overlap partially with the more narrowly defined linear array of Pb-isotope compositions associated with feldspars from Kangerlussuaq Fjord (Kn01-08, Figs. 2D, E) ∼250 km south of Disko Bugt on the western NMB and from the Kangerlussuaq Fjord System (JR106-GC06, Figs. 2C, E) from the eastern NMB (with $^{206}Pb/^{204}Pb$ values of ∼13 to 15). Feldspars sourced from Tasiilaq (525252) appear distinct in 206–207 space from our other NMB-located study regions, forming a narrowly defined linear array with relatively steep gradient between $^{206}Pb/^{204}Pb$ ratios of ∼15.5 and 16 (dark orange diamonds in Fig. 2C). These data show partial overlap with the Pb isotope composition of feldspars from Nordre Sermilik Fjord (Na04-08) in the southern KMB terrane, which are characterised by $^{206}Pb/^{204}Pb$ ratios of ∼15.5 that form tight groupings in 206–207 space with $^{207}Pb/^{204}Pb$ values of ∼15.1 (Fig. 2B).

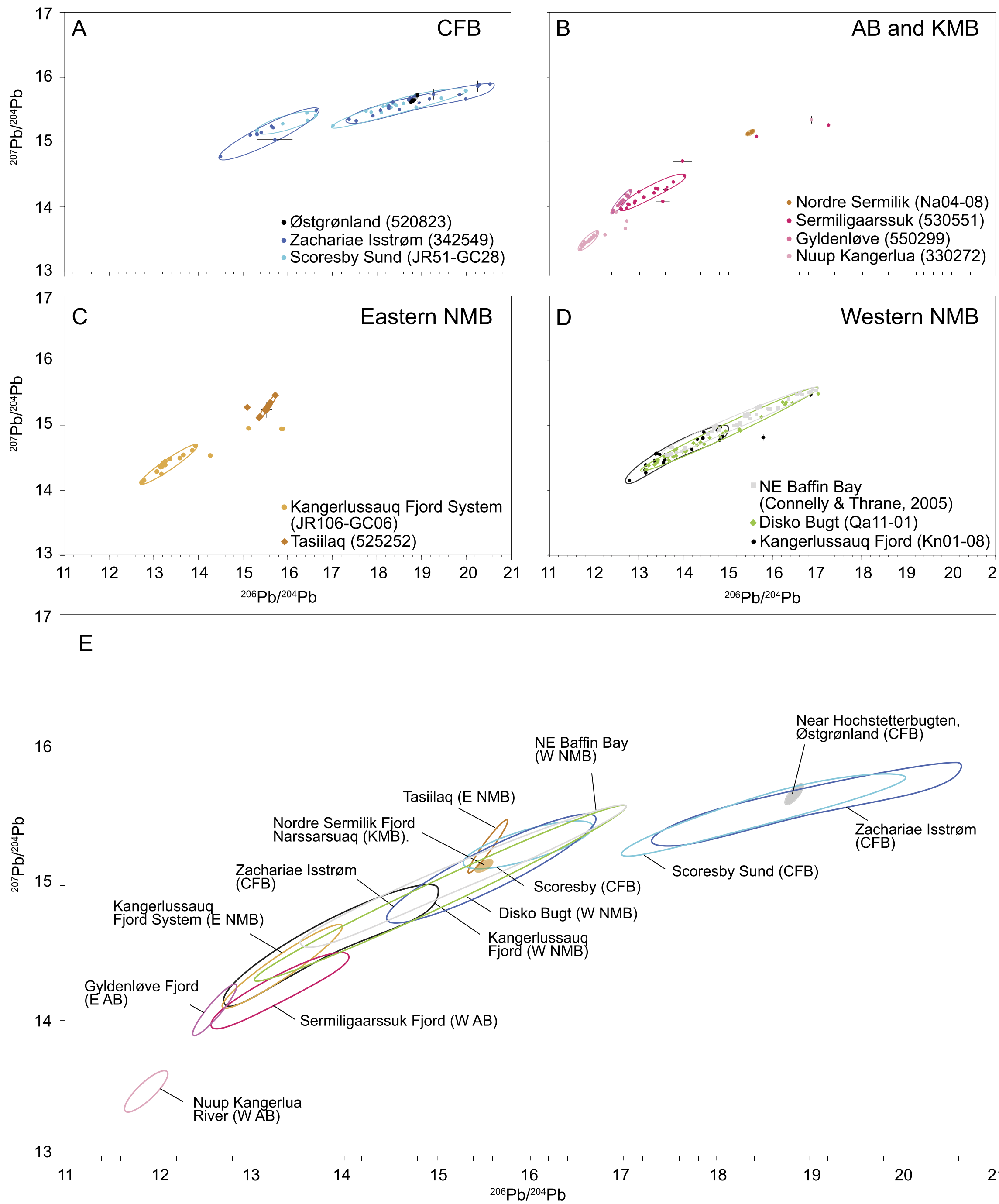

Fig. 2. The Pb-isotope composition (^{206}Pb/^{204}Pb vs. ^{207}Pb/^{204}Pb) of individual sand-sized (>150 μm) feldspars in Greenland glacifluvial and fjord sediments from localities along the coastlines of the Caledonian Fold Belt (CFB) (**A**), the Archaean Basement (AB) and Ketilidian Mobile Belt (KMB) (**B**), and the eastern (**C**) and western (**D**) Nagssugtoqidian Mobile Belt (NMB). A summary cross-plot is also presented (**E**) for the range of Pb isotope values for each sample studied. See map in Fig. 1 (and Table 1) for sample locations. Pink data (Northern domain) in (D) from Connelly and Thrane (2005) determined from replicate analysis of individual feldspars in bedrock specimens from the region north of the proposed collisional suture for the Nagssugtoqidian–Rinkian orogen within central Disko Bugt. Data >21 ^{206}Pb/^{204}Pb from Zachariae Isstrøm ($n = 2$) not shown. (For interpretation of the references to colour in this figure legend, the reader is referred to the web version of this article.)

The Pb-isotope signature of feldspars from glacifluvial sands from the western (Fig. 2B; samples 330272 and 530551) and eastern AB (Fig. 2B; sample 550299) are characterised by the least radiogenic Pb-isotope values of all individual feldspars analysed in this study and are largely distinct in 206–207 space from each other and from the provenance signature of feldspars found in NMB (Figs. 2C–D), KMB (Fig. 2B; Na04-08) and Caledonian terrane samples (Fig. 2A). On the western coast the Pb-isotope composition of feldspars from the Nuup Kangerlua River (330272) yield the lowest ^{206}Pb/^{204}Pb ratios analysed in this study (∼11.5 and ∼12.5), displaying no overlap in 206–207 space with any other analysed sample (Fig. 2E). These values agree well with the Pb-isotope composition of feldspars from Itsaq gneisses south of Isua (Kamber et al., 2003), believed to be the least radiogenic values measured anywhere on Earth and as such are unique to this area. The Pb-isotope composition of feldspars from Sermiligaarssuk Fjord (530551) are distinct from those which characterise Nuup and are well-defined by a linear array with ^{206}Pb/^{204}Pb ratios between ∼12.5 and ∼14 in 206–207 space (Fig. 2B). Similarly, the Pb-isotope composition of feldspars from Gyldenløve Fjord (550299) on the eastern coast

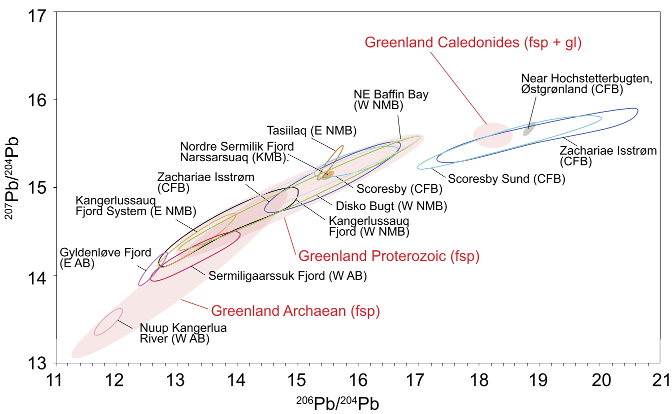

Fig. 3. Comparison of Pb-isotope values for potential Greenland ice-rafted debris sources complied by Bailey et al. (2012) (red transparent 'ellipses' and red labels) and this study (hollow multi-coloured 'bubbles' and black text labels) in ^{206}Pb/^{204}Pb–^{207}Pb/^{204}Pb space. The source fields reported in this study are based on Pb-isotope compositions of individual feldspars from Greenland glacio-fluvial and fjord sands (Fig. 2). The source fields shown from Bailey et al. (2012) are based on feldspars ('fsp') and conformable ore galenas ('gl') from circum-North Atlantic Ocean bedrock. KMB = Ketilidian Mobile Belt, E/W AB = East/West Archaean Block, W/E NMB = East/West Nagssugtoqidian Mobile Belt, CFB = Caledonian Fold Belt. (For interpretation of the references to colour in this figure legend, the reader is referred to the web version of this article.)

of the AB form a distinct narrow linear array with ^{206}Pb/^{204}Pb values between ∼12 and 13 for progressively increased values of ^{207}Pb/^{204}Pb (Fig. 2B).

4.1.2. ^{40}Ar–^{39}Ar ages of hornblendes in Greenland glacifluvial sands and fjords

The ^{40}Ar–^{39}Ar age distribution of 114 individual sand-sized hornblendes from six of our target Greenland glacifluvial sands and fjord sediments (Table 1) are shown in Fig. 4. Initial assessment of the age of individual hornblendes from these localities reveals populations characterised by a wide range of ages spanning the Palaeoarchaean to the middle Palaeozoic (∼3800 to 380 Ma) consistent with the known age distribution of Greenland's tectonic terranes (Henriksen et al., 2009). In concert with the Pb-isotope composition of feldspars from our potential IRD source regions, distinct differences exist, however, in the age distribution of hornblende grains from the individual terranes examined.

Minor numbers ($n = 5$, 21%) of hornblendes sourced from Zachariae Isstrøm (342549), the only locality in this study from the CFB to be analysed by ^{40}Ar–^{39}Ar dating, appear to be characterised by both Neoarchaen to Palaeoproterozoic (2600–1900 Ma) and earliest Neoproterozoic (1000 Ma) ages (Fig. 4A). The majority ($n = 19$, 79%), however, are part of a significantly younger mode bearing Lower Palaeozoic-ages centered on ∼450 Ma, consistent with resetting by Caledonian metamorphism (Fig. 4A). Hornblendes

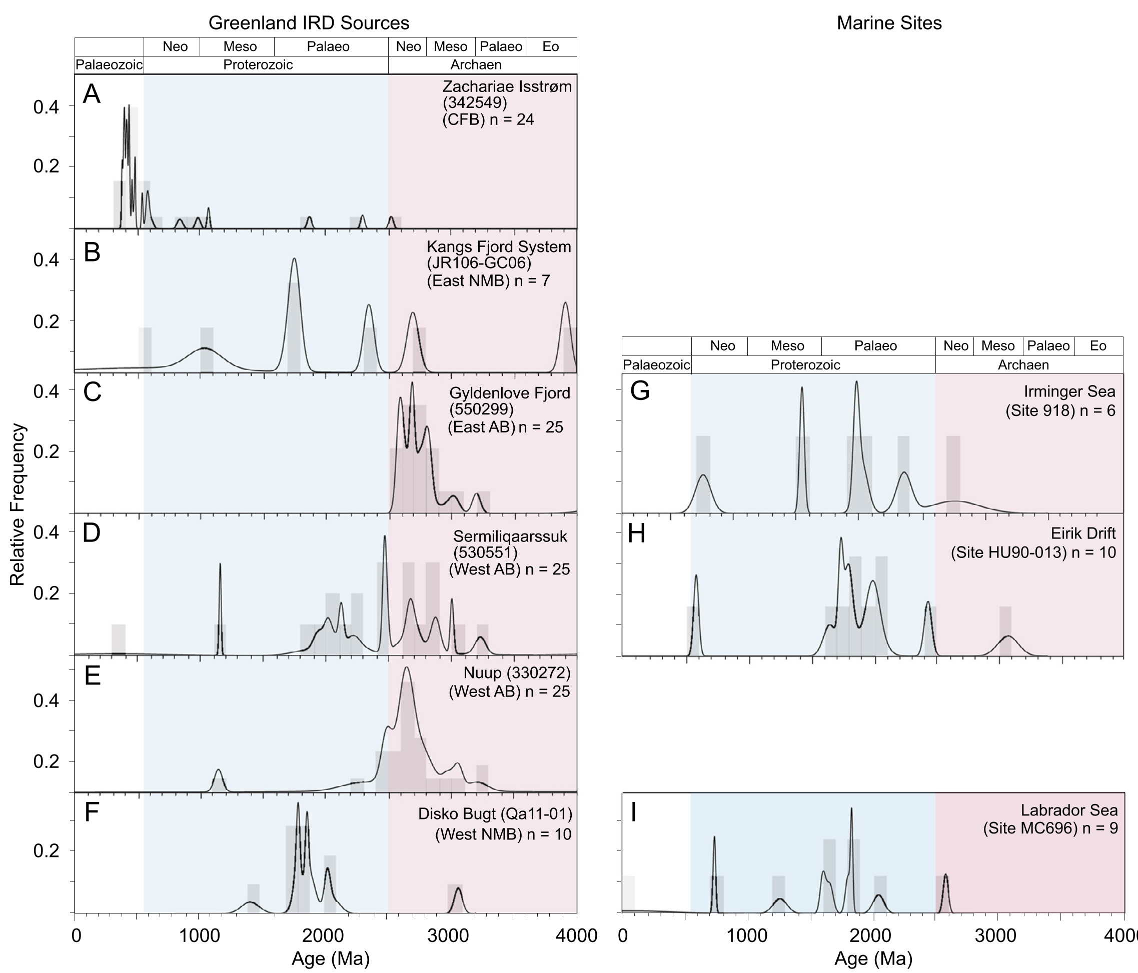

Fig. 4. Comparison of ^{40}Ar/^{39}Ar ages of individual sand-sized (>150 μm) hornblendes from Greenland glacifluvial and fjord sands (**A–F**) and Holocene Greenland-proximal marine sediments (**G–I**). Samples are ordered in terms of geographic position, starting from the north-eastern most sample (Zachariae Isstrøm, A) and moving clockwise around the GIS to the western-most samples (Disko Bugt, F). Geological timescale provided for reference. See map in Fig. 1 (and Table 1) for sample locations. CFB = Caledonian Fold Belt, NMB = Nagssugtoqidian Mobile Belt, AB = Archaean Block.

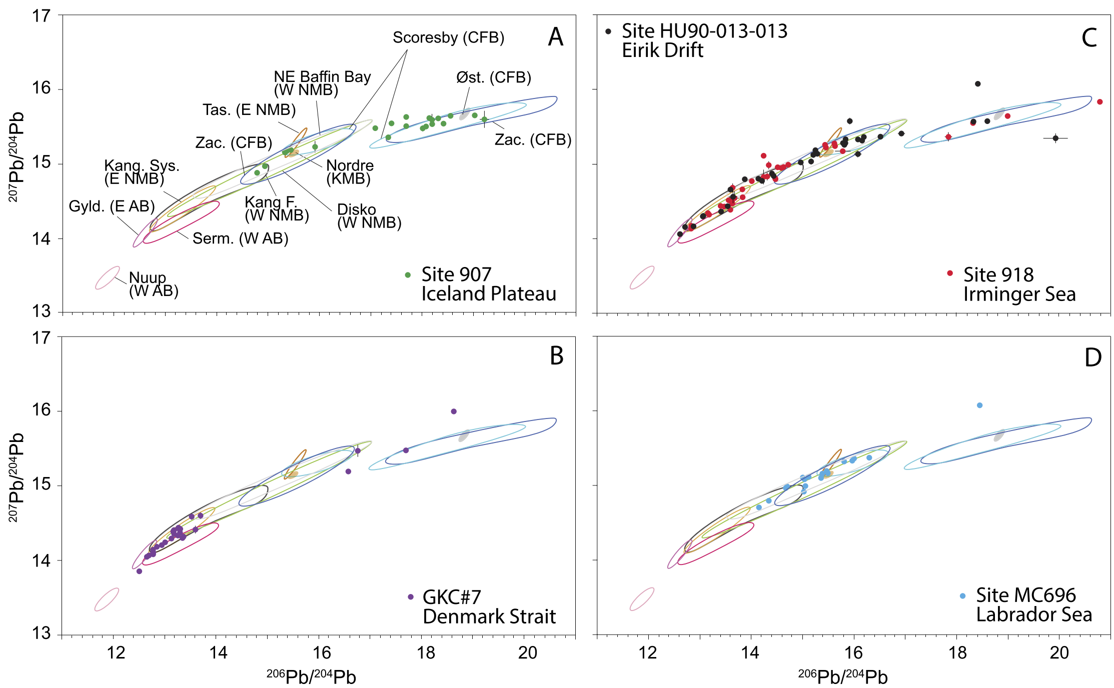

Fig. 5. Pb-isotope composition of individual sand-sized (>150 μm) feldspars from Greenland-proximal marine sediments deposited during the Holocene, highlighting spatial variation in $^{206}Pb/^{204}Pb$ vs. $^{207}Pb/^{204}Pb$. Crosses centered on individual data represent their respective 2σ uncertainties in Pb–Pb space. Where no cross is evident, uncertainties are smaller than the width of symbol used. Feldspars measured from ODP Sites 907 (**A**) and 918 (**C**) were deposited, respectively, during the Early Holocene (∼10 ka) and Middle Holocene (∼6 ka) (see Table 1). Feldspars measured from Sites GKC#7(**B**), MC696 (**D**) and HU90-013-013 (**A**) deposited during the modern or latest Holocene (see Table 1). See Fig. 2 for data used to define 'source bubbles' shown in all panels. Øst. = Østgrønland, Zac. = Zachariae Isstrøm, Scoresby = Scoresby Sund Fan, Disko = Disko Bugt, Tas. = Tasiilaq, Serm = Sermiligaarssuk Fjord, Gyld. = Gyldenløve Fjord, Nuup = Nuup Kangerlua River, Kang Sys. = Kangerlussuaq Fjord System, Kang. F = Kangerlussuaq Fjord, Norde. = Nordre Sermilik Fjord Narssarsuaq, KMB = Ketilidian Mobile Belt, E/W AB = East/West Archaean Block, E/W NMB = East/West Nagssugtoqidian Mobile Belt, CFB = Caledonian Fold Belt. Data >21 $^{206}Pb/^{204}Pb$ from Sites 918 ($n = 3$) and 907 ($n = 1$), indicative of CFB sources, not shown. (For interpretation of the references to colour in this figure, the reader is referred to the web version of this article.)

from Disko Bugt (Qa11-01) in the western KMB ($n = 10$) appear to be dominated by ages centered on ∼1800–1900 Ma (Fig. 4F). Although the hornblende population analysed is too small to be statistically significant, the five grains dated from sediments deposited in the Kangerlussuaq Fjord System (Fig. 4B, JR106-GC06) highlight that hornblendes from this important modern-day iceberg calving source may have a similar age distribution to those transported by icebergs from Disko Bugt.

Targeted AB localities are characterised by sands populated largely by Archaean hornblendes (Figs. 4C–E). Hornblendes from Gyldenløve Fjord (Fig. 4C, 550299) and Nuup Kangerlua River (Fig. 4E, 330272) on the eastern and western AB coastlines are dominated by a single skewed mode centered on ∼2600–2700 Ma. This mode is also present in the hornblende population examined from Sermiligaarssuk Fjord (530551) on the AB, although it is less prominent at this western locality because the ages of these grains exhibit a bimodal distribution that is also characterised by the presence of a second younger mode centered on ∼2100 Ma (Fig. 4D).

4.2. Provenance of IRD deposited in Greenland-proximal sediments during the Holocene

To examine how we can use our source data to reconstruct the provenance of Greenland-proximal IRD deposition, the provenance of IRD from five Greenland-proximal marine sites deposited during the early Holocene to the modern has been studied. The Pb-isotope compositions of 144 individual sand-sized feldspars deposited from these sites are shown in Fig. 5. To aid provenance determination, histograms of $^{206}Pb/^{204}Pb$ ratios for both source and marine core feldspars are shown in Fig. 6. The $^{40}Ar/^{39}Ar$ ages of 28 individual sand-sized hornblendes deposited on the Iceland Plateau (at ODP Site 918), on Eirik Drift (Site HU-90-013-013) and the Labrador Sea (Site MC-696) are also shown in Figs. 4G–I. Our analysis of the provenance of IRD deposited at these sites is primarily based on the observation that inter-terrane differences in the Pb isotope composition of ice-rafted feldspars (i.e. between those sourced from the NMB, CFB and AB) is larger than intra-terrane differences (between those sourced from individual localities studied here from, e.g. Kangerlussuaq Fjord (System) and Disko Bugt in the NMB). Based on the present-day westward ocean current system around southern Greenland we also assume that eastern IRD sources can imprint provenance signatures on sediment deposited off western Greenland whilst the opposite cannot be true. While such currents may also introduce sea-ice-derived sand sourced from the Arctic to our samples, if such detritus dominated IRD deposition at our study sites we would expect to find a lack of spatial heterogeneity in our provenance data (the opposite of what we find; see Fig. 2E and Fig. 4).

4.2.1. Site 907, Iceland Plateau

The majority of feldspars ($n = 15$; 75%) deposited at Site 907 on the Iceland Plateau during the Early Holocene form a linear array in 206–207 space with $^{206}Pb/^{204}Pb$ values ∼17–19, although a subset ($n = 5$; 25%) also cluster between values of ∼15 and 16 (Fig. 5A). In terms of provenance, this bi-modal distribution fits most closely in 206–207 space with the Pb-isotope signature of CFB-derived IRD (Fig. 5A). Our Site 907 sample contains small numbers of sand-sized basalt clasts that could have been recirculated northwards from Iceland, from the Geikie Plateau calved from the southern coastline Scoresby Sund and/or from further north at Hold With Hope and Shannon Ø. Given both the strength of the EGC today, the modelled southerly drift directions east of Greenland for icebergs sourced north of Scoresby Sund (Bigg et al., 1996) and potential for small amounts of this ice to drift further southeast prompting recirculation to the site by the northerly Irminger

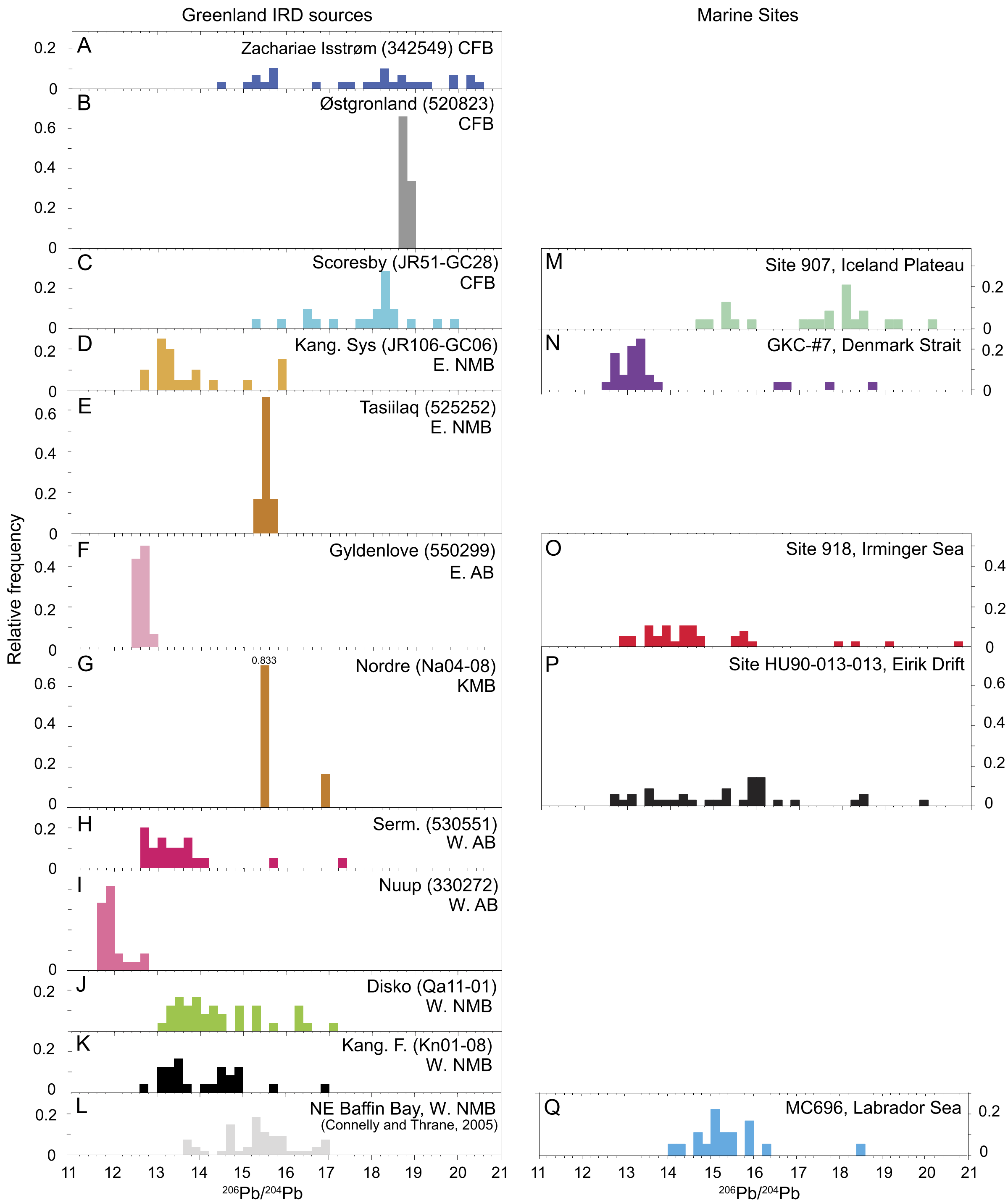

Fig. 6. Comparison of histograms of the ^{206}Pb/^{204}Pb ratios of individual sand-sized (>150 μm) feldspars from Greenland glacifluvial and fjord sands (**A–L**) and Holocene Greenland-proximal marine sediments (**M–Q**). Histograms displayed based on geographic position of samples studied: starting from the north-eastern most locality (Zachariae Isstrøm, A) moving clockwise around Greenland to the western-most localities (Disko Bugt, L). See map in Fig. 1 (and Table 1) for sample locations. CFB = Caledonian Fold Belt, E/W NMB = East/West Nagssugtoqidian Mobile Belt, E/W AB = East/West Archaean Block. (For interpretation of the references to colour in this figure, the reader is referred to the web version of this article.)

Current (i.e. Andrews et al., 2014a), we speculate that IRD deposited at Site 907 during the Early Holocene is more likely to be dominated by Caledonian sources located along the coastline of northeast Greenland.

4.2.2. Site GKC#7, Denmark Strait

Site GKC#7 lies on the Kangerlussuaq Trough margin, ∼4.5° south of Scoresby Sund (Fig. 1). Radiogenic ε_{Nd} and Sr isotope studies (Simon, 2007) of terrigenous sediments from this area show that bulk IRD deposited here bears an early Tertiary basalt signature. A subordinate number of the individual sand-sized feldspars deposited at this site in the modern (over past 150 years) are characterised by ^{206}Pb/^{204}Pb ratios >∼16 and therefore may be sourced from the CFB (Fig. 5B). The Pb-isotope compositions of the majority of feldspar from this site ($n = 24$; 86%), however, form tight clusters in 206–207 space with ^{206}Pb/^{204}Pb ratios of ∼12.5 to 13.5 (Figs. 5B and 6N). In terms of provenance, these grains mainly overlap in 206–207 space with a variety of western and eastern NMB river sands and fjord sediments (Fig. 5B). Given the location of Site GKC#7 (Fig. 1) and the strength of the EGC, the nearby Kangerlussuaq Ford System (JR106-GC06) is, however, the most likely source for these grains (Figs. 6D, N). This finding is in keeping with both the significant number of sand-sized basalt clasts (∼5–10% of assemblage) observed in our GKC#7 sample, and an XRD-based study of the bulk provenance of the <2 mm terrigenous fraction at nearby Site MD99 2322 (Fig. 1), which shows that 90% of modern-day sediments deposited at this site are sourced locally (Andrews et al., 2014a).

4.2.3. Site 918, western Irminger Sea

Although Site 918 is situated in the western Irminger Basin immediately proximal to Greenland's AB (Fig. 1), the Pb-isotope composition of only 2 of the middle Holocene feldspars (out of 35) deposited at this site (red data in Fig. 5C) overlap with analyses of glacifluvial feldspars from this tectonic terrane (e.g. from Sermiligaarssuk Fjord, 530551). Instead, their Pb-isotope compositions overlap mainly with those of feldspars from the Palaeoproterozoic NMB (Fig. 5C). $^{40}Ar/^{39}Ar$ data from Site 918 are too few in number ($n = 4$) to allow us to identify likely specific sources of IRD deposition at this site (Fig. 4G). Yet their Palaeoproterozoic ages (∼1870–2250 Ma) tentatively support the notion that Site 918 IRD is dominantly sourced from the NMB (Fig. 4B) and not from local eastern AB sources (Fig. 4C). The provenance inferred for Site 918 IRD based on these data is consistent with eastern NMB and CFB sources inferred for drop stones from nearby grab station DS97-18 (Linthout et al., 2000) and with the relatively high abundance (∼5–10%) of sand-sized basalt found in our sample. Given the presence of small numbers of grains in our Site 918 feldspar population that are unambiguously derived from Caledonian sources ($n = 4$), it is possible that some of the 'NMB' feldspars might instead represent 'far-travelled' IRD sourced from the CFB.

4.2.4. Site HU90-013-013, Eirik Drift

Many of the feldspars deposited on Eirik Drift at Site HU90-013-013 during the latest Holocene exhibit a similar distribution in 206–207 space to those deposited up-current at Site 918 (compare black and red data in Figs. 5C and 6G, and $^{206}Pb/^{204}Pb$ histograms in Figs. 6O, P). This finding implies that many of the sources responsible for IRD deposition in the western Irminger Basin during the middle Holocene are also responsible for IRD deposition on Eirik Drift during the latest Holocene. The Pb-isotope composition of two feldspars deposited at Site HU90-013-013 highlight a potential, albeit minor, contribution from sediments shed from the eastern AB to IRD deposition at this site during the modern (two black data in Fig. 4C that overlap with Gyldenløve Fjord Pb-isotope values). In support of this concept, $^{40}Ar/^{39}Ar$ data from this site highlight that at least some hornblendes deposited on Eirik Drift are Archaean in age (Fig. 4H).

The absence of any sand-sized basalt clasts in our Site HU90-013-013 sample argues against the eastern NMB being the dominant source for feldspars deposited at this site during the latest Holocene. A number of feldspars deposited at Site HU90-013-013 with $^{206}Pb/^{204}Pb$ ratios between ∼15 and 17 ($n = 13$) do not overlap with Pb-isotope data from Site 918 in 206–207 space (Fig. 5C). The absence of feldspars with such compositions in our Site 918 dataset indicates that these grains may not be sourced from east Greenland. Both iceberg trajectory modelling (Bigg et al., 1996) and analysis of Landsat imagery (Howat and Eddy, 2011) suggest that these feldspars may represent grains derived from important modern-day iceberg calving sources located on the KMB yet to be documented in our source datasets.

4.2.5. Site MC-696, Labrador Sea

The location of Site MC-696 in the Labrador Sea permits iceberg calving locations from all of Greenland's tectonic terranes to be potential sources of IRD deposition at this site (Fig. 1). It is notable, therefore, that feldspars deposited at this site during the modern are largely characterised by Pb-isotope compositions that are only likely to be derived from either the NMB or KMB (blue data in Figs. 5D and 6Q). A number of these grains ($n = 12$) also overlap in 206–207 space with the Pb-isotope composition of feldspars from the CFB (Fig. 5D). Indeed, one data point with a high $^{206}Pb/^{204}Pb$ ratio (of ∼18) implies that some icebergs calved from this region apparently survive the journey to the Labrador Sea (Figs. 5D and 6Q). Potential north-western sources (i.e. the Petermann glacier) are known to generate icebergs capable of reaching the Labrador sea (Halliday et al., 2012). Whilst ice drift models suggest both sources (north of Denmark Strait and NW Greenland) are marginally capable of supplying Site MC-696 (Bigg et al., 1996), the absence of large numbers of grains with a CFB signature makes it highly unlikely that the majority of feldspars deposited at Site MC-696 with unambiguous $^{206}Pb/^{204}Pb$ ratios (∼15–16) are sourced from these far-field regions.

Owing to overlap between Proterozoic sources of Greenland IRD in 206–207 space it is not currently possible to determine the origin of most feldspars deposited at Site MC-696 at the intra-terrane scale. Their Pb-isotope compositions arguably show good agreement in 206–207 space with NMB iceberg calving sources in Kangerlussuaq Fjord (Kn01-08), Disko Bugt (Qa11-01) and the region to its north (Connelly and Thrane, 2005) (Fig. 5D). These data are also comparable in 206–207 space with the composition of feldspars deposited on Eirik Drift (HU90-013-013) with $^{206}Pb/^{204}Pb$ ratios ∼15–17 that we attribute to KMB iceberg calving (compare Figs. 5C to 6D, H).

4.3. Inferences on Holocene GIS retreat based on Greenland sand IRD provenance data

A reconstruction of the Holocene evolution of GIS iceberg calving sources based on our new datasets is beyond the scope of this study. Yet, the provenance determinations that can be made for both our new and previously published (e.g. Knutz et al., 2013) Holocene Greenland-proximal marine IRD datasets based on our new characterisations for Greenland-sourced IRD demonstrate the potential that this approach has to provide valuable context on previous inferences of the retreat history of the GIS during the Early Holocene (e.g. Bennike and Björck, 2002; Dyke et al., 2014; Winsor et al., 2015).

For instance, the Pb isotope composition of sand-sized feldspars that we report for Site 907 indicate that northeast Greenland was still supplying IRD to the Iceland Plateau at ∼10 ka, which is consistent with the ^{14}C chronology for the timing (∼10–9 ka before present) for deglaciation of the coastal margin of northeast Greenland during the Early Holocene (Bennike and Björck, 2002). Based on ^{10}Be surface exposure ages and ^{14}C chronologies from the coastline of southwest Greenland it has been inferred that on the western AB, the GIS retreated rapidly from the coastline towards its near-modern ice margin between ∼11 and 10 ka (Bennike and Björck, 2002; Winsor et al., 2015). Indeed, our Pb isotope and Ar–Ar data from Site MC-696 (64°N, 57.6′W) show that the western AB does not represent a modern source of IRD to the adjacent Labrador Sea (compare Figs. 7A and C). Recent evidence for significant deposition of Archaean ice-rafted hornblendes at Site DA04-31 (62.3°N, 54.2′W) during the Early Holocene (Knutz et al., 2013) suggest, however, that the outlet glaciers on the western AB remained a significant source of IRD to the Labrador Sea until at least ∼9 ka, which our Greenland source characterisation indicates was most likely derived from the Nuuk region (the Godthåbsfjord and

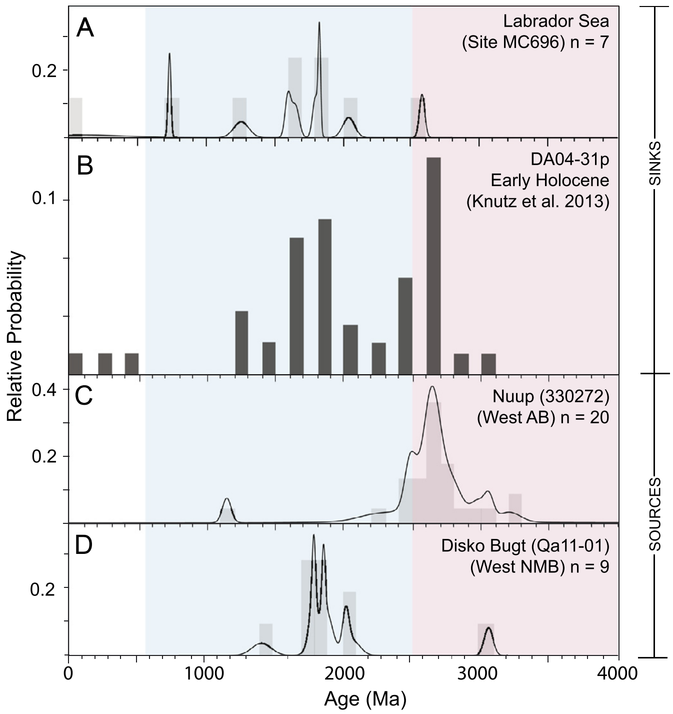

Fig. 7. Comparison of $^{40}Ar/^{39}Ar$ ages of individual sand-sized (>150 μm) hornblendes from Holocene Greenland-proximal marine sediments within the Labrador Sea deposited both in the modern (**A**; this study) and Early Holocene, 9–11 ka (Knutz et al., 2013); **B**). $^{40}Ar/^{39}Ar$ ages from potential western NMB and AB terrane sources (**C–E**).

Buksejford systems; compare Figs. 7B and C). Limited data exist that track GIS retreat on the eastern AB during the Early Holocene. The absence of AB-sourced IRD deposition at Site 918 at ∼6 ka is consistent with the picture based on ^{10}Be exposure ages of glacial erractics that Bernstorffs Fjord in SE Greenland was deglaciated by ∼10.4 ka (Dyke et al., 2014). Alternatively, the dominance of feldspars and hornblendes deposited at Site 918 at ∼9 ka with an NMB signature, may suggest that major glacier outlets from the eastern NMB represented the dominant source of iceberg and IRD generation in the Early Holocene as they do today.

5. Conclusions

We present new records of the Pb-isotope composition of individual sand-sized feldspars and the $^{40}Ar/^{39}Ar$ ages of individual sand-sized hornblendes from modern Greenland glacifluvial river and fjord sands and Holocene Greenland-proximal marine sediments. Our new datasets demonstrate for the first time that the Pb-isotope composition of sand-sized feldspars and $^{40}Ar/^{39}Ar$ ages of sand-sized hornblendes glacially eroded by the GIS exhibit distinct spatial differences, that spatial heterogeneity exists in sources of IRD deposited in Greenland-proximal marine sediments and that it is possible to determine the source(s) of Greenland IRD at the terrane scale. Significant overlap exists in the provenance signature of IRD derived from a range of important modern-day point specific sources on both the east Caledonian Fold Belt (e.g. Scorseby Sund and Zachariae Isstrøm) and the western (e.g. Disko Bugt) and eastern (e.g. Kangerlussuaq Fjord System) Nagssugtoqidian Mobile Belt. Our new source datasets reveal, however, that Pb isotope and Ar–Ar age data has great potential to pin down the provenance signature of IRD derived from intra-terrane point specific sources within Greenland's Achaean Basement. The provenance that we infer for our marine IRD samples is consistent with an Early Holocene timing for deglaciation of the coastal margins of southern Greenland. The generation of such datasets from sand-sized hornblendes and feldspars therefore has great potential to help better understand spatial differences in the provenance of IRD deposited in the Greenland-proximal marine setting and the timing of southern GIS margin deglaciation during the Holocene and past interglacials.

Acknowledgements

This research used marine samples provided by (I)ODP, which was sponsored by the US National Science Foundation and participating countries under management of Joint Oceanographic Institutions, Inc. We thank W. Hale and A. Wuelbers at Bremen for help with sampling and J.A. Milton, R.M. Jones, J. Hughes and M.R. Spencer at Southampton for laboratory assistance. We also thank N. Keulen, K. Thrane (GEUS) and A.V. Reyes (Dublin) for providing the Greenland river sands used in this study and M. Kuchera (Bremen) and A. de Vernal (UQÀM) for providing sediment from marine Sites MC696 and HU-90-013-013, respectively. This manuscript was greatly improved by the constructive comments of three anonymous reviewers and editor D. Vance. Funding for this project was provided by NERC grant NE/H014187/1 (C.D.S). Acquisition of cores JR51-GC28 and JR106-GC06 was supported by UK NERC grants GST/02/2198 and NER/T/S/2000/00986 (J.A.D).

Appendix A. Supplementary material

Supplementary material related to this article can be found online at http://dx.doi.org/10.1016/j.epsl.2015.10.054.

References

Adams, C.J., Kelley, S.P., 1988. Provenance of Permian–Triassic and Ordovician metagraywacke terranes in New Zealand: evidence from $^{40}Ar–^{39}Ar$ dating of detrital micas. Geol. Soc. Am. Bull. 110, 422–432. http://dx.doi.org/10.1130/0016-7606(1998)110<0422:POPTAO>2.3.CO;2.

Alonso-Garcia, M., Andrews, J.T., Belt, S.T., Cabedo-Sanz, P., Darby, D., Jaeger, J., 2013. A multi-proxy and multi-decadal record (to AD 1850) of environmental conditions on the East Greenland shelf (∼66°N). Holocene 23, 1672–1683.

Andrews, J.T., 2011. Unravelling sediment transport along glaciated margins (the Northwestern Nordic Seas) using quantitative X-ray diffraction of bulk (<2 mm) sediment. In: Bhuiyan, A.F. (Ed.), Sediment Transport. InTech, pp. 225–248.

Andrews, J.T., Bigg, G.R., Wilton, D.J., 2014a. Holocene sediment transport from the glaciated margin of East/Northeast Greenland (67–80°N) to the N Iceland shelves: detecting and modeling changing sediment sources. Quat. Sci. Rev. 91, 204–217.

Andrews, J.T., Gibb, O.T., Jennings, A.E., Simon, Q., 2014b. Variations in the provenance of sediment from ice sheets surrounding Baffin Bay during MIS 2 and 3 and export to the Labrador Shelf Sea: site HU2008029-0008 Davis Strait. J. Quat. Sci. 29, 3–13.

Andrews, J.T., Vogt, C., 2014. Source to sink: statistical identification of regional variations in the mineralogy of surface sediments in the western Nordic Seas (58°N–75°N; 10°W–40°W). Mar. Geol. 357, 151–162. http://dx.doi.org/10.1016/j.margeo.2014.08.005.

Bailey, I., Foster, G.L., Wilson, P.A., Jovane, L., Storey, C.D., Trueman, C.N., Becker, J., 2012. Flux and provenance of ice-rafted debris in the earliest Pleistocene subpolar North Atlantic Ocean comparable the last glacial maximum. Earth Planet. Sci. Lett. 341–344, 222–233. http://dx.doi.org/10.1016/j.epsl.2012.05.034.

Bailey, I., Hole, G.M., Foster, G.L., Wilson, P.A., Storey, C.D., Trueman, C.N., Raymo, M.E., 2013. An alternative suggestion for the Pliocene onset of major northern hemisphere glaciation based on the geochemical provenance of North Atlantic Ocean ice-rafted debris. Quat. Sci. Rev. 75, 181–194. http://dx.doi.org/10.1016/j.quascirev.2013.06.004.

Bennike, O., Björck, S., 2002. Chronology of the last recession of the Greenland Ice Sheet. J. Quat. Sci. 17, 211–219.

Bierman, P.R., Corbett, L.B., Graly, J.A., Neumann, T.A., Lini, A., Crosby, B.T., Rood, D.H., 2014. Preservation of a preglacial landscape under the center of the Greenland Ice Sheet. Science 344, 402–405.

Bigg, G.R., Wadley, M.R., Stevens, D.P., Johnson, J.A., 1996. Prediction of iceberg trajectories for the North Atlantic and Arctic Oceans. Geophys. Res. Lett. 23 (4), 3587–3590.

Bindoff, N.L., Stott, P.A., AchutaRao, K.M., Allen, M.R., Gillett, N., Gutzler, D., Hansingo, K., Hegerl, G., Hu, Y., Jain, S., Mokhov, I.I., Overland, J., Perlwitz, J., Sebbari, R., Zhang, X., 2013. Detection and attribution of climate change: from global to regional. In: Stocker, T.F., Qin, D., Plattner, G.-K., Tignor, M., Allen, S.K., Boschung, J., Nauels, A., Xia, Y., Bex, V., Midgley, P.M. (Eds.), Climate Change 2013: The Physical Science Basis. Contribution of Working Group I to the Fifth Assessment Report of the Intergovernmental Panel on Climate Change. Cambridge University Press, Cambridge, United Kingdom and New York, NY, USA.

Carlson, A.E., Winsor, K., 2012. Northern hemisphere ice-sheet responses to past climate warming. Nat. Geosci. 5, 607–613. http://dx.doi.org/10.1038/NGEO1528.

Connelly, J.N., Thrane, K., 2005. Rapid determination of Pb isotopes to define Precambrian allochthonous domains: an example from West Greenland. Geology 33, 953–956.

Cook, C.P., Hill, D.J., van de Flierdt, T., Williams, T., Hemming, S.R., Dolan, A.M., Pierce, E.L., Escutia, C., Harwood, D., Cortese, G., Gonzales, J.J., 2014. Sea surface temperature control on the distribution of far-traveled Southern Ocean ice-rafted detritus during the Pliocene. Paleoceanography 29. http://dx.doi.org/10.1002/2014PA002625.

Dawes, P.R., 2009. The bedrock geology under the Inland Ice: the next major challenge for Greenland mapping. Geol. Surv. Den. Greenl. Bull. 17, 57–60.

Dethleff, D., Kuhlmann, G., 2009. Entrainment of fine-grained surface deposits into new ice in the southwestern Kara Sea, Siberian Arctic. Cont. Shelf Res. 29, 691–701.

Dowdeswell, J.A., Evans, J., Ó Cofaigh, C., 2010. Submarine landforms and shallow acoustic stratigraphy of a 400 km-long fjord-shelf-slope transect, Kangerlussuaq margin, East Greenland. Quat. Sci. Rev. 29, 3359–3369.

Dyke, L.M., Hughes, A.L.C., Murray, T., Hiemstra, J.F., Andresen, C.S., Rodes, A., 2014. Evidence for the asynchronous retreat of large outlet glaciers in southeast Greenland at the end of the last glaciation. Quat. Sci. Rev. 99, 244–259.

Gilotti, J.A., Jones, K.A., Elvevold, S., 2008. Caledonian metamorphic patterns in Greenland. In: Higgins, A.K., Gilotti, J.A., Smith, M.P. (Eds.), The Greenland Caledonides: Evolution of the Northeast Margin of Laurentia. In: Mem. Geol. Soc. Amer., vol. 202, pp. 201–225.

Grocott, J., Pulvertaft, T.C.R., 1990. The Early Proterozoic Rinkian belt of central West Greenland. In: Lewry, J.F., Stauffer, M.R. (Eds.), The Early Proterozoic Trans-Hudson Orogen of North America. In: Spec. Pap., Geol. Assoc. Can., vol. 37, pp. 443–463.

Gwiazda, R.G., Hemming, S.R., Broecker, W.S., 1996. Tracking the sources of icebergs with lead isotopes: the provenance of ice-rafted debris in Heinrich layer 2. Paleoceanography 11, 77–93. http://dx.doi.org/10.1029/95PA03135.

Halliday, E.J., King, T., Bobby, P., Copland, L., Mueller, D., 2012. Petermann Ice Island 'A' Survey Results, Offshore Labrador. In: OTC Arctic Technology Conference.

Hemming, S.R., Broecker, W.S., Sharp, W., Gwiazda, R., McManus, J.F., Klas, M., Hajdas, I., 1998. Provenance of Heinrich layers in core V28-82, northeastern Atlantic: ^{40}Ar/^{39}Ar ages of ice-rafted hornblende, Pb isotopes in feldspar grains, and Nd–Sr–Pb isotopes in the fine sediment fraction. Earth Planet. Sci. Lett. 164, 317–333. http://dx.doi.org/10.1016/S0012-821X(98)00224-6.

Henriksen, N., Higgins, A.K., Kalsbeek, F., Pulvertaft, T.C.R., 2009. Greenland from Archaean to Quaternary. Descriptive Text to the 1995 Geological Map of Greenland, 1:2 500 000, 2nd edition. Geol. Surv. Den. Greenl. Bull., vol. 18, 126 pp.

Hogan, K.A., Dowdeswell, J.A., Ó Cofaigh, C., 2012. Glacimarine sedimentary processes and depositional environments in an embayment fed by West Greenland ice streams. Mar. Geol. 311, 1–16. http://dx.doi.org/10.1016/j.margeo.2012.04.006.

Howat, I.M., Eddy, A., 2011. Multi-decadal retreat of Greenland's marine-terminating glaciers. J. Glaciol. 57 (8), 389–396. http://dx.doi.org/10.3189/002214311796905631.

Jansen, E., Fronval, T., Rack, F., Channell, J.E.T., 2000. Pliocene–Pleistocene ice rafting history and cyclicity in the Nordic Seas during the last 3.5 Myr. Paleoceanography 15 (6), 709–721. http://dx.doi.org/10.1029/1999PA000435.

Kalsbeek, F., Higgins, A.K., Jepsen, H.F., Frei, R., Nutman, A.P., 2008. Granites and granites in the East Greenland Caledonides. In: Higgins, A.K., Gilotti, J.A., Smith, M.P. (Eds.), The Greenland Caledonides: Evolution of the Northeast Margin of Laurentia. In: Mem. Geol. Soc. Amer., vol. 202, pp. 227–249.

Kamber, B.S., Collerson, K.D., Moorbath, S., Whitebouse, M.J., 2003. Inheritance of early Archaean Pb-isotope variability from long-lived Hadean protocrust. Contrib. Mineral. Petrol. 145, 25–36. http://dx.doi.org/10.1007/s00410-002-0429-7.

Knutz, P.C., Sicre, M.A., Ebbesen, H., Christiansen, S., Kuijpers, A., 2011. Multiple-stage deglacial retreat of the southern Greenland Ice Sheet linked with Irminger Current warm water transport. Paleoceanography 26, 1–18. http://dx.doi.org/10.1029/2010PA002053.

Knutz, P.C., Storey, M., Kuijpers, A., 2013. Greenland iceberg emissions on strained by ^{40}Ar/^{39}Ar hornblende ages: implications for ocean-climate variability during last deglaciation. Earth Planet. Sci. Lett. 375, 441–449.

Knutz, P.C., Hopper, J.R., Gregersen, U., Nielsen, T., Japsen, P., 2015. A contourite drift system on the Baffin Bay–West Greenland margin linking Pliocene Arctic warming to poleward ocean circulation. Geology 43, 907–910.

Linthout, K., Troelstra, S.R., Kuijpers, A., 2000. Provenance of coarse ice-rafted detritus near the SE Greenland margin. Neth. J. Geosci. 79 (1), 109–121.

Meehl, G.A., Stocker, T.F., Collins, W.D., Friedlingstein, P., Gaye, A.T., Gregory, J.M., Kitoh, A., Knutti, R., Murphy, J.M., Noda, A., Raper, S., Watterson, A.J., Weaver, Z.C., Zhao, C., 2007. Global climate projections. In: Solomon, S., Qin, D., Manning, M., Chen, Z., Marquis, M., Averyt, K.B., Tignor, M., Miller, H.L. (Eds.), Climate Change 2007: The Physical Science Basis. Contribution of Working Group I to the Fourth Assessment Report of the Intergovernmental Panel on Climate Change. Cambridge University Press, Cambridge, United Kingdom and New York, NY, USA.

Mitrovica, G.X., Gomez, N., Clark, P.U., 2009. The sea-level fingerprint of West Antarctic Collapse. Science 323, 753. http://dx.doi.org/10.1126/science.1166510.

Morlighem, M., Rignot, E., Mouginot, J., Seroussi, H., Larour, E., 2014. Deeply incised submarine glacial valleys beneath the Greenland ice sheet. Nat. Geosci. 7, 418–422. http://dx.doi.org/10.1038/NGEO2167.

Nielsen, T., Kuijpers, A., 2013. Only 5 southern Greenland shelf edge glaciations since the early Pliocene. Nat. Sci. Rep. 3, 1875. http://dx.doi.org/10.1038/srep01875.

North Greenland Ice Core Project Members (NGRIP), 2004. High-resolution record of Northern Hemisphere climate extending into the last interglacial period. Nature 431, 147–151. http://dx.doi.org/10.1038/nature02805.

Otto-Bliesner, B.L., Marshall, S.J., Overpeck, J.T., Miller, G.H., Hu, A., et al., 2006. Simulating Arctic climate warmth and icefield retreat in the Last Interglaciation. Science 311, 1751–1753. http://dx.doi.org/10.1126/science.1120808.

Pfirman, S.L., Colony, R., Nürnberg, D., Eicken, H., Rigor, I., 1997. Reconstructing the origin and trajectory of drifting Arctic sea ice. J. Geophys. Res. 102 (12), 575–12586.

Renne, P.R., Swisher, C.C., Deino, A.L., Karner, D.B., Owens, T.L., DePaolo, D.J., 1998. Intercalibration of standards and absolute ages and uncertainties in ^{40}Ar/^{39}Ar dating. Chem. Geol. 145, 117–152. http://dx.doi.org/10.1016/S0009-2541(97)00159-9.

Reyes, A.V., Carlson, A.E., Beard, B.L., Hatfield, R.G., Stoner, J.S., Winsor, K., Welke, B., Ullman, D.J., 2014. South Greenland ice-sheet collapse during Marine Isotope Stage 11. Nature 510, 525–528. http://dx.doi.org/10.1038/nature13456.

Rignot, E., Braaten, D., Gogineni, S.P., Krabill, J., McConnell, J.R., 2004. Rapid ice discharge from southeast Greenland Glaciers. Geophys. Res. Lett. 31, L10401. http://dx.doi.org/10.1029/2004GL019474.

Rignot, E., Kanagaratnam, P., 2006. Changes in the velocity structure of the Greenland ice sheet. Science 311, 986–990. http://dx.doi.org/10.1126/science.1121381.

Rignot, E., Mouginot, J., 2012. Ice flow in Greenland for the International Polar Year 2008–2009. Geophys. Res. Lett. 39, L11501. http://dx.doi.org/10.1029/2012GL051634.

Sherlock, S.C., 2001. Two-stage erosion and deposition in a continental margin setting: an ^{40}Ar/^{39}Ar laserprobe study of offshore detrital white micas in the Norwegian Sea. J. Geol. Soc. 158, 793–799. http://dx.doi.org/10.1144/0016-7640001-021.

Simon, Q., 2007. Analyse sédimentologique et isotopique (Nd & Pb) d'une carotte sédimentaire prélevée dans le Détroit du Danemark (MD99-2322) Implication sur l'évolution de la circulation océanique profonde au cours de l'Holocène. Oceanography, Liege, 92.

St John, K.E.K., Krissek, L.A., 2002. The late Miocene to Pleistocene ice-rafting history of southeast Greenland. Boreas 31, 28–35. http://dx.doi.org/10.1111/j.1502-3885.2002.tb01053.x.

Strachan, R.A., Martin, M.E., Friderichsen, J.D., 2001. Evidence for contemporaneous yet contrasting styles of granite magmatism during extensional collapse of the northeast Greenland Caledonides. Tectonophysics 20, 458–473. http://dx.doi.org/10.1029/2000TC001206.

Tang, C.C.L., Ross, C.K., Yao, T., Petrie, B., DeTracey, B.M., Dunlap, E., 2004. The circulation, water masses and sea–ice of Baffin Bay. Prog. Oceanogr. 63 (4). http://dx.doi.org/10.1016/j.pocean.2004.09.005.

Thiede, J., Jessen, C., Knutz, P., Kuijpers, A., Mikkelsen, N., Nørgaard-Pedersen, N., Spielhagen, R.F., 2011. Millions of years of Greenland Ice Sheet history recorded in ocean sediments. Polarforschung 80 (3), 141–159. hdl:10013/epic.38391.d001.

Valeur, H.H., Hansen, C., Hansen, K.Q., Rasmussen, L., Thingvad, N., 1996. Weather, sea and ice conditions in eastern Baffin Bay, offshore northwest Greenland, a review. Danish Met. Institute Tech. Report Number 96-12.

Vernal, A., Hillaire-Marcel, C., 2000. Sea-ice cover, sea-surface salinity and halo-/thermocline structure of the northwest North Atlantic: modern versus full glacial conditions. Quat. Sci. Rev. 19, 65–85.

Wartho, J.-A., Kelley, S.O., Brooker, R.A., Carroll, M.R., Villa, I.M., Lee, M., 1999. Direct measurement of Ar diffusion profiles in a gem-quality Madagascar K-feldspar using the ultra-violet laser ablation microprobe (UVLAMP). Earth Planet. Sci. Lett. 170, 141–153. http://dx.doi.org/10.1016/S0012-821X(99)00088-6.

Weidick, A., 1995. In: Williams, R.S., Ferrigno, J. (Eds.), Satellite Image Atlas of the Glaciers of the World: Greenland. U.S. Geol. Surv. Prof. Pap. 1386-C. 153 pp.

Weidick, A., Bennike, O., 2007. Quaternary glaciation history and glaciology of Jakobshavn Isbræ and the Disko Bugt region, West Greenland: a review. Geol. Surv. Den. Greenl. Bull. 14, 78.

Winsor, K., Carlson, A.E., Caffee, M.W., Rood, D.H., 2015. Rapid last-deglacial thinning and retreat of the marine-terminating southwestern Greenland ice sheet. Earth Planet. Sci. Lett. 426, 1–12. http://dx.doi.org/10.1016/j.epsl.2015.05.040.